Journal of the European Ceramic Society 43 (2023) 7656–7667

Contents lists available at ScienceDirect

Journal of the European Ceramic Society

journal homepage: www.elsevier.com/locate/jeurceramsoc

High temperature oxides for selective absorption of thermal radiation

Victor K. Champagne III *, Giovanni Pisaturo, David R. Clarke

School of Engineering and Applied Sciences, Harvard University, Boston, MA 02134, United States

ARTICLE INFO

Keywords:
Thermal radiation
Rare-earth zirconates
Dieke diagram
Substitutional doping
Minimum thermal conductivity

ABSTRACT

Most high melting temperature oxides are translucent in the visible-infrared region characteristic of the black-body thermal radiation at high temperatures. Consequently, over this broad-band spectral region, the "thermal radiation window", they do not absorb thermal radiation. Translucent oxides, such as the zirconates, can be extensively doped with rare-earth (RE) ions (Nd, Sm, Er, Dy, Yb) to achieve selective spectral absorption, and the doped oxides exhibit low thermal conductivity. The optical absorption bands are due to electronic transitions between electronic states associated with the rare-earth ions and are relatively insensitive to other rare-earth ions within the same compound. Therefore, mixed rare-earth compounds exhibit optical absorption characteristic of the sum of the individual ions' absorptions. By contrast, the thermal conductivity of the RE zirconates is shown to be relatively independent of composition suggesting that their optical properties in the thermal radiation window regions can be modified without affecting their thermal conduction properties.

1. Introduction

Most thermal absorbers are materials that absorb thermal radiation over a wide spectral range, for instance those designed to capture the thermal radiation from a black body radiator, such as the sun, or used in quantifying absorption, such as in calibrating thermal cameras. These are typically electronic conductors and, to suppress reflectivity, they are used in the form of very rough surfaces, as assemblies of small particles, fibrous or highly porous, convoluted structures. Common examples are carbon black paint or black silicon, the latter a heavily etched phosphorus-doped silicon [1]. There is also interest in using selective absorption pigments in paints for altering the temperature of walls and roofs [2]. For space vehicles, materials with different surfaces have been developed for either increasing their black body absorbance or, conversely, their reflectance. With the advent of concentrated solar power, there has been an increased interest in developing highly absorbing surfaces and particles [3] that can operate at high temperatures in air since oxidation invariably occurs in concentrated solar systems. Less common as thermal absorbers are high-temperature materials, such as oxides, that exhibit highly selective absorption, meaning that they absorb strongly at specific phonon and wavelength energies (wavelengths) but not at others. At high temperatures, these oxides might be designed to absorb radiation from specific molecules in a hot combustion gas, for instance water vapor or carbon dioxide. Conversely, they might be used as selective filters, allowing transmission at specific wavelengths, but absorbing others for enhancing signal-to-noise in transmission. In this contribution, we describe the use of rare-earth doping in otherwise translucent, refractory oxides, such as zirconia and zirconates, to create selective thermal radiation absorbers stable at very high temperatures. Combined with their low thermal conductivities, these oxides may have application in reducing the total heat flux through coatings used in gas turbine engines [4].

Most oxides that are stable in air at high temperatures, for instance, at 800 °C and above, are usually referred to as insulators, but they are also wide-band gap semiconductors. Consequently, they do not absorb over the optical spectrum from the visible to mid-infra-red [5] where the majority of thermal radiation flux from high-temperatures sources lies. This might be termed the thermal radiation window. Because of this intrinsic transparency, many oxides are used as optical and infra-red windows [5,6]. For instance, as shown in Table 1, many high-purity single crystals and silica glass do not absorb until at least 4.5 μm [5]. (Their polycrystalline counterparts generally appear white primarily because of scattering from entrained porosity although grain boundary scattering can also contribute to absorption in optically anisotropic materials because of refractive index changes across the grain boundaries). It is also well known that point defects like oxygen vacancies lead to light absorption in otherwise transparent materials such as oxides: in a reducing atmosphere, zirconia will turn black upon exposure at elevated temperatures. However, this type of coloration is not stable in an oxidizing environment like the one found in a gas turbine engine or

* Corresponding author.
E-mail address: vchampagne@g.harvard.edu (V.K. Champagne III).

https://doi.org/10.1016/j.jeurceramsoc.2023.07.075
Received 15 May 2023; Received in revised form 14 July 2023; Accepted 28 July 2023
Available online 3 August 2023
0955-2219/© 2023 Elsevier Ltd. All rights reserved.

Table 1
The optical transmittance cut-off of common refractory oxides and calculated high-temperature minimum thermal conductivity.

Material	Optical transmittance cutoff*[13]) (μm)	Calculated high temperature minimum thermal conductivity ** (W/m*K)
Quartz and Fused Silica (SiO_2)	4.5	1.11
ALON ($9Al_2O_3{\cdot}5AlN$)	5.5	2.56
Spinel ($MgAl_2O_4$)	6	2.36
Sapphire (Al_2O_3)	6	2.81
Zirconia (ZrO_2)	6	1.39
Yttria (Y_2O_3)	8	1.21
Magnesium Oxide (MgO)	8.5	2.52

** Using Eq. 2.
* Defined as the wavelength at which a 2 mm thick sample has 10% optical transmittance [13]

concentrated solar absorber. Substitutional doping with a transition element ion or a rare-earth ion is known to introduce color by absorption [7,8]. For instance, the Cr^{3+} ion can substitute for an Al^{3+} ion in the crystal structure of sapphire to give both the well-known red color of ruby and sharp emission bands with characteristic R1, R2 doublet at 693.53 nm and 692.12 nm [9,10]. Similarly, YAG is transparent, but when doped with Sm^{3+} appears yellow in color. It also emits several sharp emission lines due to electronic transitions when excited in the green or blue. Indeed, the sharp emission lines from such transition element ions and rare-earth dopants in oxides have been the basis for the development of a wide variety of high-power lasers in which the populations of electronic transitions can be inverted by pumping. Similarly, doped oxide-based phosphors, for excitation by electron beams, and more recently, UV emissions from GaN-based LEDs and lasers have paved the way for the development of solid-state lighting. While doped oxides (and nitrides and oxynitrides) are examples of selective absorbers, the attainable concentration of dopants is limited to optimize frequency conversion and minimize heating. For instance, in most cases, self-absorption of the emitted light leads to concentration quenching [11]. In other cases, the concentration is limited by the strain-induced distortion associated with the dopant size mismatch to its host, leading to emission broadening. For selective thermal absorbers, these limitations are less restrictive since it is not desired to maximize their emission. This not only allows for higher doping concentrations but also simultaneous doping by multiple different ions. The maximum doping concentration is then typically dictated by the solubility of the ions in the crystal structure of the chosen host oxide.

In this work, we demonstrate that substitutional doping of a variety of refractory but transparent oxides by rare-earth ions can produce optical absorption, over the spectral range of high-temperature black-body thermal radiation, without affecting their high-temperature thermal conductivity.

2. Material design concepts

In designing dopant strategies for producing compositions that exhibit selective optical absorption in the thermal radiation window, we have been primarily guided by two bodies of literature. One is the well-established literature describing the origins of optical transitions of ions in crystalline hosts using crystal field theory [14,15], and embodied, for instance, in the Dieke diagrams for the lanthanide ions in solution [16]. The other are the rules of crystal chemistry, which determine how the solubility of a substitutional ion in a crystalline host is determined by its ionic radius, valence and coordination, largely based on Pauling's rules [17,18]. Much of this data is compiled in the tables presented in reference [19].

Transitions between 4*f*-4*f* transitions in the Ln^{3+} ions are particularly attractive as selective absorbers since they are sharp and spectrally narrow [14]. In addition, the transitions from partially filled 4*f* electron orbital states are shielded by the outer *5s* to *6s* electron orbitals. Hence, they are less sensitive to changes in the local atomic environment, for instance due to lattice strains or being in solution in different crystal structures. Although the transitions between the 4*f*-5*d* states of the Ln^{2+} ions, such as Yb^{2+} and Sm^{2+} ions, are generally much broader and can be more intense they require the stabilization of the reduced valence state in an oxidizing environment if the oxide is to be used in air. If co-existence of both Ln^{2+} and Ln^{3+} ions can be achieved this also gives rise to the possibility of inter-valence charge transmission (IVCT) bands as additional absorption bands. However, at high temperatures in air the Ln^{2+} ions are oxidized and, as described by [20] the blue absorption color associated with Yb^{2+} in $Yb_3Al_5O_{12}$ bleaches out with time at high temperatures. For this reason, the focus of our investigations has been on the use of trivalent lanthanides as dopants in a variety of crystalline oxide hosts.

For convenience, the Dieke diagram for the electronic levels associated with Ln^{3+} ions is reproduced [21] in Fig. 2 on which is superimposed, by shading, the range of energies corresponding to the most intense black body emission at 1700°C. Corresponding diagrams exist for Ln^{2+} ions [22]. It is evident from this comparison that although most Ln^{3+} ions exhibit one or more optical transition that can be excited by black-body radiation, some such as Gd^{3+}, cannot as they do not have energy levels in this range. This motivates the selection of compositions selected for presentation in this study. Also, evident is that most of the electronic transitions of the rare-earth ions occur at different energies and do not overlap. This motivates a second set of experiments in which the optical absorption of host oxides containing mixtures of different rare-earth ions is investigated.

The ionic radii of the trivalent rare-earth ions in six-fold coordination range, typical of their substitution in most oxides [19], range from 0.11 nm (La^{3+}) to 0.085 nm (Lu^{3+}). Several oxides with very high melting temperatures can accommodate trivalent ions in solid solution, notably the pyrochlore zirconates, aluminates, spinels, apatites, and garnets, although the cation substitutional solubility varies significantly from one crystal structure to another. Of particular interest are stabilized zirconia and many of the zirconates and hafnates, as they are known to have very low thermal conductivity above 800 °C and melt above 2500 °C. Substitution of rare-earth ions in tetragonal zirconia is limited as it requires either the formation of oxygen vacancies to maintain charge neutrality or co-substitution with a pentavalent ion, such as Nb^{5+} or Ta^{5+}. The latter enable an extended range over which the transformation toughened compositions are possible [23–26], but leads to compositions that ideally are pseudo-binaries between $YTaO_4$ and ZrO_2 [27]. Nevertheless, the yttria-stabilized zirconia composition exhibits unusually large fracture toughness in the meta-stable tetragonal phase, a parameter of significance in applications subject to large cyclic thermal stresses, such as coated gas turbine blades [28,29]. Furthermore, the yttria stabilizer (Y^{3+}) can be replaced by Yb^{3+} and other rare-earth ions, such as Ce^{4+}, preserving the tetragonal phase [30] and, as will be shown, introduce dopant selective optical absorption. Another class of oxides of interest because of their high melting temperatures are the zirconates [31], one of which, $Gd_2Zr_2O_7$, is currently in commercial use as a thermal barrier coating. As suggested by their general formula, $Ln_2^{3+}Zr_2^{4+}O_7^{2-}$, the zirconates offer even greater ranges of solubility, in some cases complete solid solution between the endmember compounds, for instance $(Gd_{1-x}Yb_x)_2 \quad Zr_2 \quad O_7$. Furthermore, there are two distinct crystallographic sites in both the pyrochlore zirconate structure and fluorite ordered structure for trivalent ions, one with a six-fold coordination and the other with an eight-fold coordination. Consequently, they provide an opportunity to explore the effect of alternative doping approaches over a larger range of solubilities.

The effect of dopant ions on the thermal conductivity of oxides is

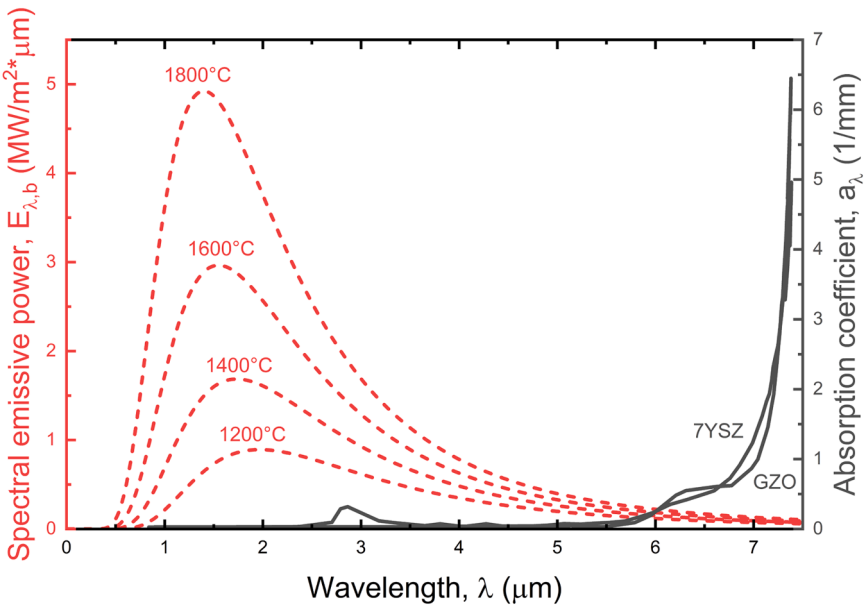

Fig. 1. Comparison between the black body power spectral distribution (dashed), at the indicated temperatures, and the spectral region over which yttria-stabilized zirconia (7YSZ) and gadolinium zirconate (GZO) exhibit minimal absorption until ~ 7 μm. Data taken from [12].

well established [32,33]. At temperatures below about twice the Debye temperature, dopant ions that have a different atomic mass, size and/or valence can substantially lower thermal conductivity. This is generally attributed to phonon scattering from the substitutional ion and the locally strained lattice introduced by it. At significantly higher temperatures, approximately 2–3 times the Debye temperature, the effect of dopants is smaller until the thermal conductivity falls to the theoretical minimum value, κ_{min}, for a disordered crystal. This minimum value can be expressed, at high temperatures, in terms of phonon scattering [34] as:

$$\kappa_{\min} = \frac{k_B}{2.48} \quad n^{2/3} \quad (2v_T + v_L) \tag{1}$$

where k_B is the Boltzmann constant, n is the number density of atoms, and v_T and v_L are the acoustic velocities of the transverse and longitudinal phonons modes, respectively. A similar scaling expression in terms of macroscopic properties [35], that is useful if the phonon spectrum of an oxide is not known, is:

$$\kappa_{\min} = k_B \nu_m \Lambda_{\min} \rightarrow 0.87 k_B \overline{\Omega}_a^{-2/3} (E/\rho)^{1/2} \tag{2}$$

where $\overline{\Omega}$ is the mean atomic volume of the atoms in the unit cell, ν_m is the mean phonon velocity, $\Lambda_{\min}$ is the minimum phonon mean free path, ρ is the density, and E is Young's modulus.

An important feature of this minimum thermal conductivity at high temperatures is that it is an asymptotic value and so does not change with further increases in temperature. (The asymptotic behavior is primarily due to the asymptotic dependence of specific heat with increasing temperature [36] and the phonon mean free path approaching the inter-atomic spacing. Unless a new heat transfer mechanism becomes activated at higher temperatures, for instance thermally activated electronic conduction, the thermal conductivity neither increases nor decreases with further increases in temperature once the minimum thermal conductivity is attained).

3. Experimental details

The oxide materials studied were synthesized by a complexing of cations in an aqueous -organic solution and subsequent chelation [37], sometimes referred to as the modified-Pechini method. Several crystalline hosts with low thermal conductivity at high temperatures were prepared, including single phase zirconates, zirconia, silicates and aluminates, although most of the observations in this contribution were zirconates. For these batches of rare-earth zirconate powder (with a general formula, $RE_2Zr_2O_7$, where RE= Gd, Nd, Sm, Yb, Dy, Er, or some combination of these elements) and the rare-earth doped zirconium dioxide were synthesized [38]. This method was chosen over others because it results in homogeneously dispersed metal cations in the oxide. The precursors were metal salts, obtained from Strem Chemicals with a purity of 99.9%: Zirconium dichloride oxide hydrate, Gadolinium nitrate hexahydrate, Neodymium nitrate hexahydrate, Samarium nitrate hexahydrate, Ytterbium nitrate pentahydrate, Dysprosium nitrate hexahydrate, and Erbium nitrate hydrate. Solutions of each cation were prepared by dissolving each metal salt separately in deionized (DI) water and gravimetric analysis used to determine the cation concentration in solution. For each composition, stoichiometric amounts of each cation in solution were measured and stirred while heated in an oil bath maintained between 80 and 90 °C. Ethylenediaminetetraacetic acid (EDTA) (Sigma-Aldrich, BioUltra, Anhydrous, ≥99%, titration) was used as the chelating agent and mixed with the cations at a 1:1 molar ratio. The resulting solution has a low pH, so ammonium hydroxide (Sigma-Aldrich, ACS reagent, 28.0–30.0%) was added dropwise to maintain the pH between 8 and 9 and to allow the EDTA to dissolve and form stable complexes with the metal cations (visually indicated by the solution turning from cloudy to clear) without precipitating any metal hydroxides. The solution takes on the color of the rare-earth cation e.g., the Er^{3+} solution is pink and the Nd^{3+} solution is purple while remaining transparent.

Once mixed, water was allowed to evaporate until the solution became more viscous, but still pourable. It was then transferred to an alumina crucible and heated at 500 °C to evaporate the remaining water. Typically, a black foam was formed which was then crushed and calcined in air at 750 °C for two hours to remove all organic material, leaving only the oxide powder. At this stage, the powder was white with a visual hue characteristic of the absorption color of the rare-earth cation. It was lightly ground using an alumina mortar and pestle and pressed into pellets using a hardened steel die at a pressure of 200 MPa for 3 min. The pellets were sintered in air at 1500 °C for 4 h with a ramp rate of 5 °C/min. The resulting grain sizes were determined from SEM images taken of the samples by the linear intercept method and are

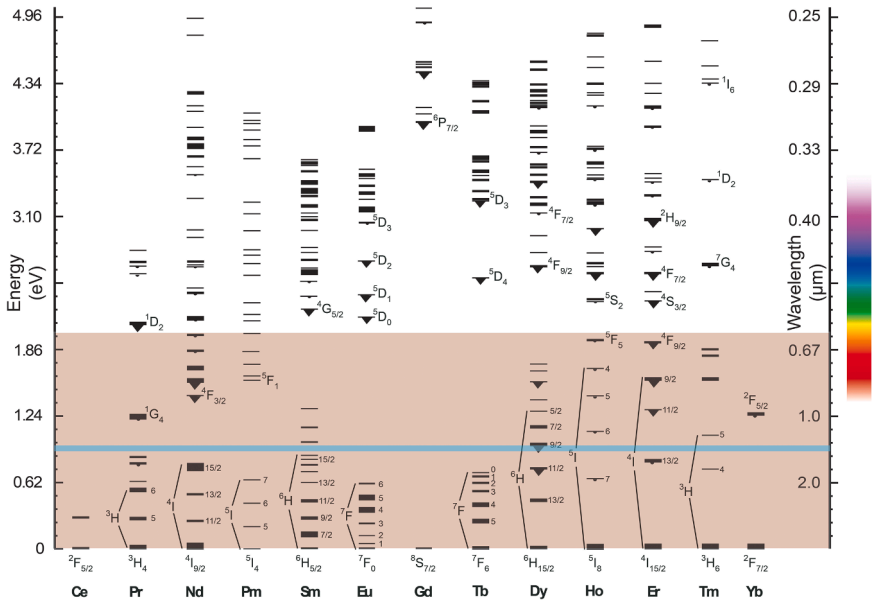

Fig. 2. The Dieke diagram [21] represents the electron energy levels associated with the individual trivalent lanthanide ions indicated. The superimposed brown band represents the approximate thermal energy of a radiating blackbody at a temperature of 1700°C (the peak temperature represented by the horizontal blue line). The diagram is for ions in solution and so does not include crystal field effects or spin splitting levels.

shown in Table A.1. The average grain size ranged from 0.30 to 0.94 μm. The sintered pellets were approximately 1 mm thick.

The optical absorption spectra were determined from hemispherical UV–VIS–NIR optical reflectance measurements of thick samples using a Hitachi U-4100 Spectrophotometer with a barium sulfate-coated integrating sphere. A Spectralon Diffuse Reflectance Standard with a reflectance factor of 99% was used for the baseline measurement. The diffuse reflectance measurements were made from wavelengths of 400 nm to 2500 nm, encompassing most of the spectral range of radiative emissions likely from very hot objects (Fig. 1). The use of the integrating sphere results in an effective instrumental broadening of about 40 nm, calibrated from measurements of single crystals. The reflectance data was subsequently used to determine values of the spectral optical absorption (K) and scattering coefficients (S) using the Kubelka-Munk method [39,40]. According to this method, the ratio K/S can be obtained from the diffuse reflectance, R_∞, recorded from very thick samples [39] as:

$$\frac{(1-R_\infty)^2}{2R_\infty} = \frac{K}{S} \tag{3}$$

and the scattering coefficient, S, [39] is:

$$S = \frac{1}{h}\frac{R_\infty}{(1-R_\infty)} \tag{4}$$

where h is the thickness of the sample.

In addition, optical spectroscopy measurements were made using continuous laser excitation to verify the dopants were in solid solution within the crystalline hosts. These measurements were complemented by X-ray diffraction analysis to confirm the materials were single phase and for determination of the lattice parameters.

The thermal diffusivity as a function of temperature up to 990 °C was measured using a standard laser flash method [41] in argon using a Netzsch LFA 457 instrument. This commercial instrument uses a milli-second Nd glass laser pulse to heat the front side of a circular disk sample and an InSb IR detector to monitor the temperature of the back side as a function of time following the laser pulse. Both the front and back sides of the sample were coated with carbon to ensure absorption of the laser to create a thermal pulse at the front and the back side with carbon to provide a surface with an emissivity of unity. The thickness of the carbon coating was chosen to prevent any laser penetrating through the sample; any penetration typically shows up in the thermogram as an immediate jump in detector voltage after the laser pulse is triggered. An example of the optical laser penetration is given in figure 7 of reference [33]. The thermal conductivity was calculated from the measured thermal diffusivity values using the equation:

$$k = \alpha c_p \rho \tag{5}$$

where k is the thermal conductivity, α is the thermal diffusivity, c_p is the specific heat, and ρ is the density. The theoretical density was determined by a Rietveld analysis of the powder XRD patterns, and the bulk density was measured by Archimedes' method. The specific heat was calculated from the Kopp-Neumann Law using specific heat data for oxides from [42–44], and, for the Sm and Nd zirconates, compared to values from Fabrichnaya et al. [45]. In those two compounds, there was less than 6% difference at low temperatures and less than 1% at 1000°C.

The measured thermal conductivity was corrected for porosity using the standard Maxwell relation [35], which assumes that the pores are closed and uniformly distributed, to give a value of the fully dense material in terms of the volume fraction, ϕ, of porosity:

$$k_{dense} = k_{measured} \quad \frac{1}{1-1.5\varnothing} \tag{6}$$

The values of thermal conductivity for the fully dense oxides reported in this work are the measured values after correction for porosity, typically < 15%. The relative densities are shown in Table A.1 for each of the RE zirconate samples.

4. Results

4.1. Optical absorption

Fig. 3a compares the absorption spectrum as a function of Yb^{3+} concentration across the solid solution $(Gd_{1-x}Yb_x)_2ZrO_7$ series. The absorption coefficients, computed from the Kubelka-Munk analysis of the reflectance data, are shown in Fig. 3b. As expected from the electronic energy levels represented in the Dieke diagram, there is no absorption in the $Gd_2Zr_2O_7$ material since neither the Gd^{3+} nor the Zr^{4+} ions have allowed excited states between 500 nm and 5.0 mm. There is,

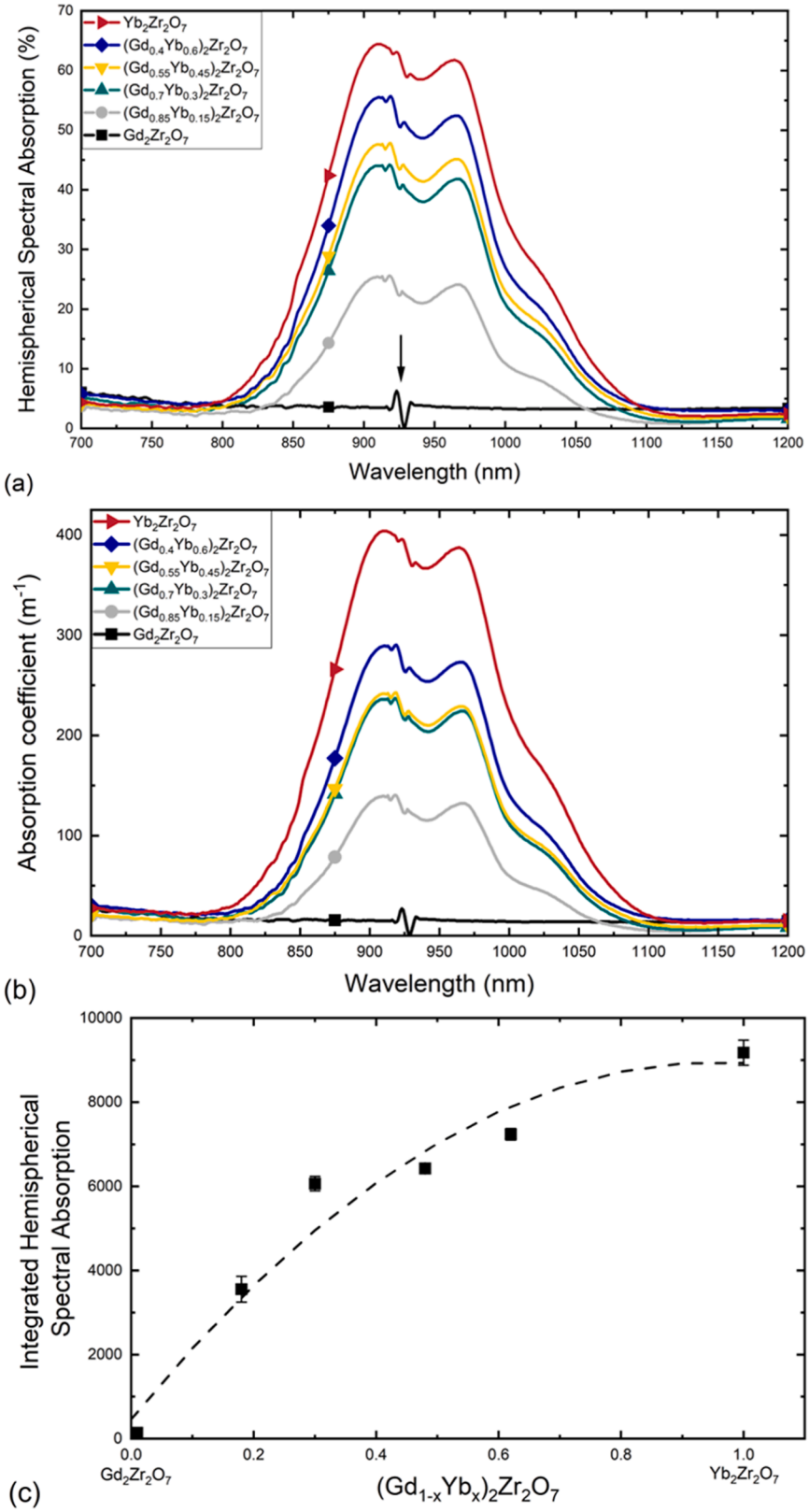

Fig. 3. (a) Hemispherical spectral absorption as a function of incident wavelength of a range of solid solution compositions as Yb replaces Gd in $Gd_2Zr_2O_7$. As expected from the electronic energy levels in the Dieke diagram for the Gd and Yb ions, there is no absorption for the $Gd_2Zr_2O_7$ compound, and the absorption increases with increasing Yb^{3+} concentration until the endmember $Yb_2Zr_2O_7$ compound. The arrow indicates an instrumental artifact associated with detector switching which is also evident in the absorption bands. (b) The absorption coefficients as a function of Yb concentration. (c) The integrated hemispherical spectral absorption vs. composition plot shows the relationship between the addition of Yb and the resulting increase in absorption.

however, an absorption band centered at about 950 nm which is associated with $^2F_{7/2} - {}^2F_{5/2}$ transitions in the Yb^{3+} ions. Strikingly, the observed absorption is a broad doublet with a high wavelength shoulder rather than a single absorption peak typical of absorption by Yb^{3+} ions in Yb-doped zirconia and YAG. As mentioned earlier, the instrumental broadening is ~ 40 nm so the unusual breadth, ~ 200 nm, is concluded to be due to local strain and polycrystalline effects. (The spectral fine details in Yb-containing compounds, [46] [47], associated with crystal field and spin splitting as well as vibronic effects are not resolved). Comparison of the spectra in the $(Gd_{1-x}Yb_x)_2ZrO_7$ series shows (Fig. 3c)

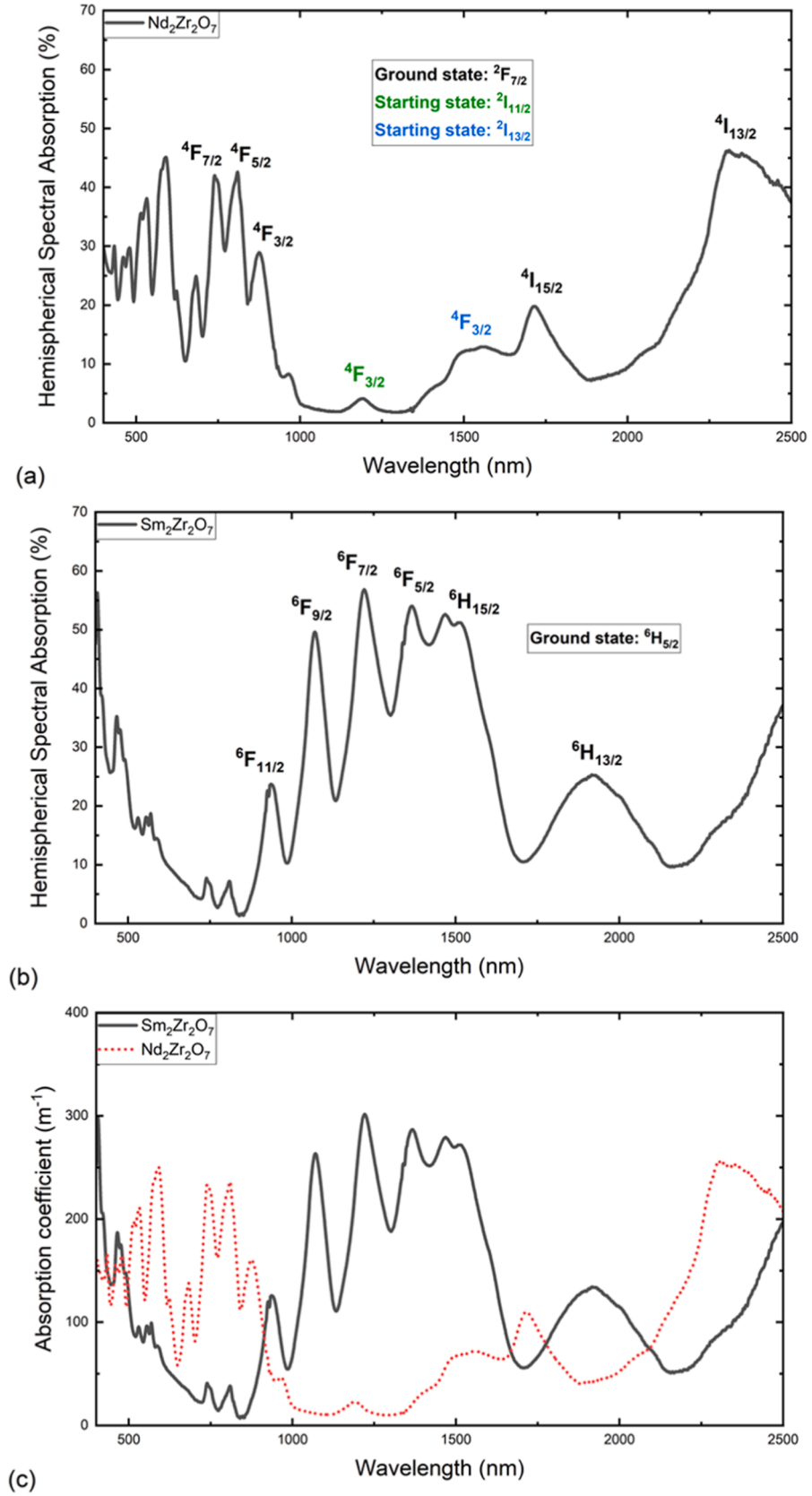

Fig. 4. The hemispherical spectral absorption of sintered polycrystalline $Nd_2Zr_2O_7$ (a) and $Sm_2Zr_2O_7$ (b) with the principal electronic transitions indicated. (c) The derived absorption coefficients of the two materials.

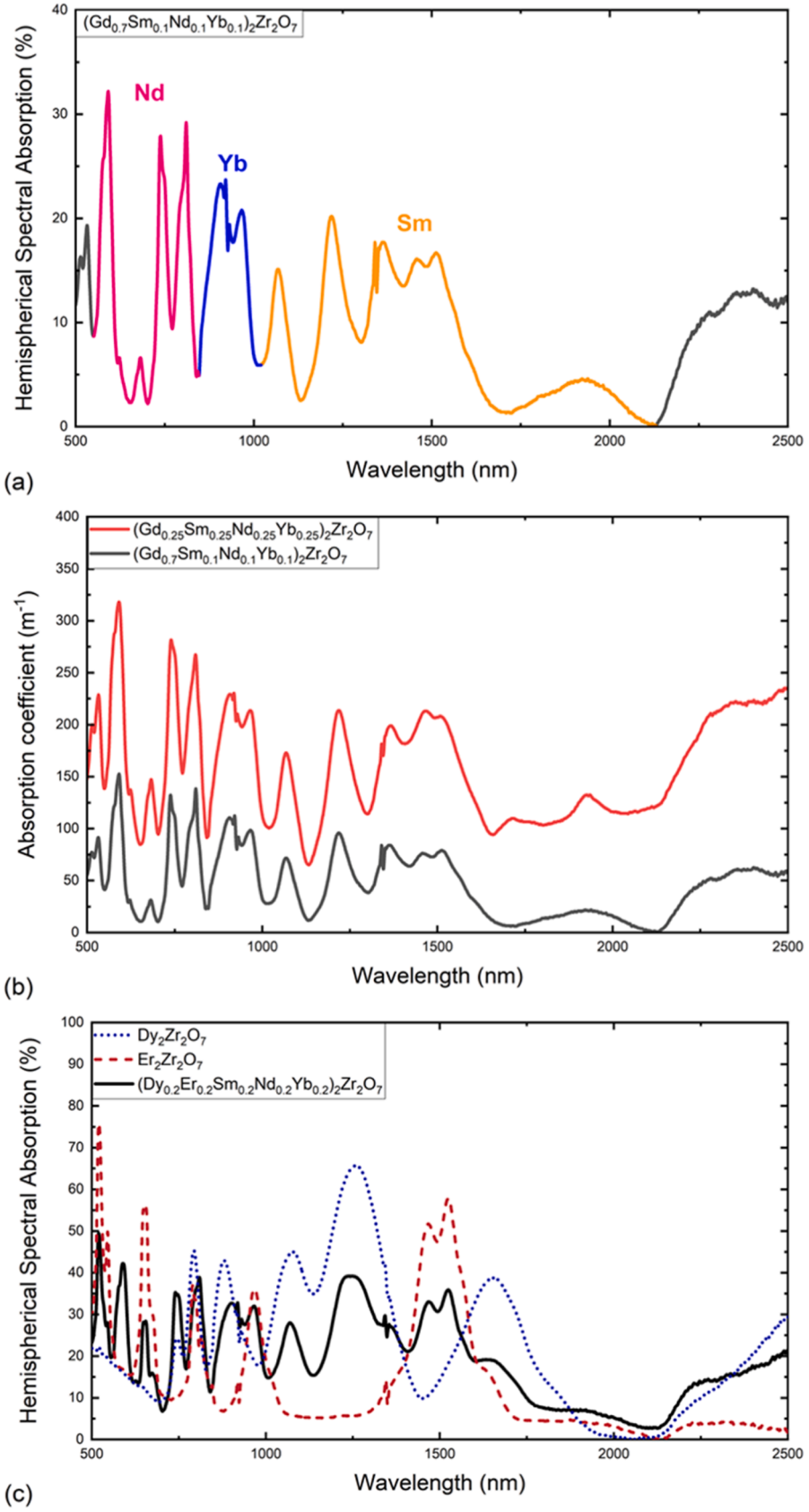

Fig. 5. (a) Hemispherical spectral absorption for equal mixtures of Sm, Nd, Yb ions substituted into $Gd_2Zr_2O_7$. The spectral contributions from the individual rare-earth ions are indicated in color. (b) The corresponding absorption coefficients for $(Gd_{0.7}Sm_{0.1}Nd_{0.1}Yb_{0.1})_2Zr_2O_7$ and $(Gd_{0.25}Sm_{0.25}Nd_{0.25}Yb_{0.25})_2Zr_2O_7$. (c) Absorption spectra of $(Dy_{0.2}Er_{0.2}Sm_{0.2}Nd_{0.2}Yb_{0.2})_2Zr_2O_7$ which shows the individual contributions from the rare-earth ions Dy^{3+} and Er^{3+}.

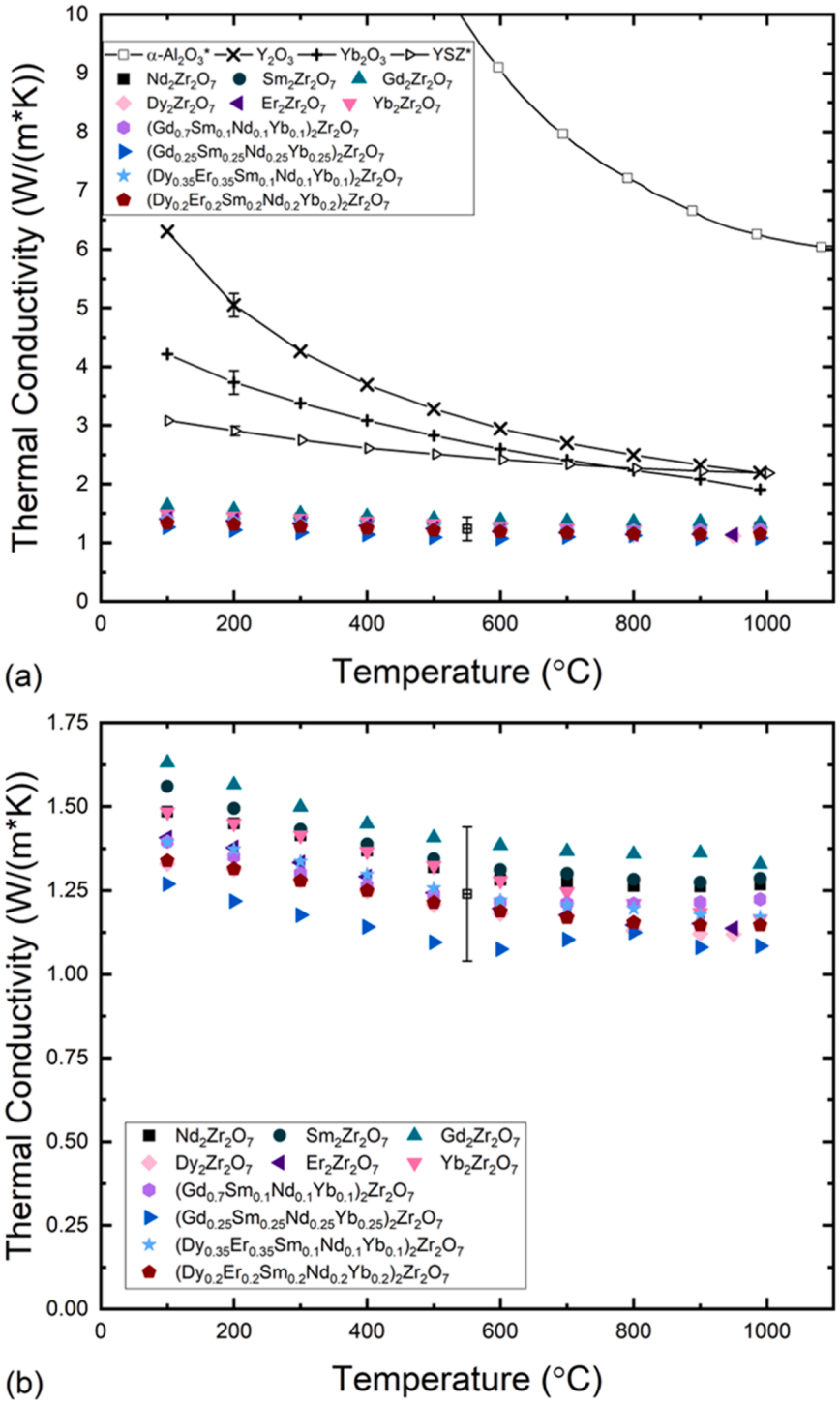

Fig. 6. (a) Thermal conductivity as a function of. temperature for the single rare-earth zirconate end members and mixed rare-earth zirconate solid solutions measured with laser flash method. For comparison, the conductivity data for other oxides with the corundum crystal structure, Y_2O_3, Yb_2O_3 and Al_2O_3 (data from [50]), are shown as well as for yttria-stabilized tetragonal zirconia (data from [51]). (b) The conductivity of the zirconates showing that all of them, including the high entropy zirconate, are indistinguishable given the measurement uncertainty of the laser flash measurements, shown by the error bar.

that the absorption increases in proportion to the Yb^{3+} ion concentration up to the compound $Yb_2Zr_2O_7$, the end member of the solid solution series.

Other compounds containing Yb^{3+} also exhibit absorption over a similar range of wavelength centered around 950 nm, namely Yb stabilized ZrO_2, Yb_2O_3, Yb_2SiO_5 (monosilicate), $Yb_2Si_2O_7$ (disilicate) and Yb-doped $Y_3Al_5O_{12}$ (YAG) as illustrated by the hemispherical absorption spectra shown in the Appendix. The absorption spectra of these materials all exhibit absorption that is associated with the Yb^{3+} ion, indicating a relative insensitivity to the host lattice. However, as expected, there is a slight difference in position and intensity of the absorption peaks due, presumably, to differences in the Yb^{3+} ions positions in the host lattices. Most notably, though, is that the spectra are all doublets except for the $Y_3Al_5O_{12}$ (YAG) crystals.

Fig. 4(a) is a comparison of the absorption spectra for the Sm and Nd zirconates, $Sm_2Zr_2O_7$ and $Nd_2Zr_2O_7$. As with the $(Gd_{1-x}Yb_x)_2ZrO_7$ series, each of the absorption lines can be attributed to the possible electronic energy levels for excitation from their respective ground states. The absorption spectra are also similar to the reported reflectance spectra for the Sm_2O_3 and Nd_2O_3 oxides [48]. The values of the derived spectral absorption coefficients are shown in Fig. 4c.

As the optical absorption associated with the tri-valent rare-earth

Table 2
Thermal conductivities of the RE zirconates.

Composition	XRD Density (kg/m^3)	Measured Thermal Conductivity at 990°C (W/m*K)	Calculated minimum thermal conductivity (W/m*K)
$Nd_2Zr_2O_7$	6400 [52]	1.27	1.17
$Sm_2Zr_2O_7$	6650 [53]	1.29	1.16
$Gd_2Zr_2O_7$	6950	1.33	1.15
$Dy_2Zr_2O_7$	7270 [54]	1.12	1.15
$Er_2Zr_2O_7$	7470 [54]	1.14	1.14
$Yb_2Zr_2O_7$	7710	1.17	1.13
$(Gd_{0.7}Nd_{0.1}Sm_{0.1}Yb_{0.1})_2Zr_2O_7$	6900	1.22	1.15
$(Gd_{0.25}Nd_{0.25}Sm_{0.25}Yb_{0.25})_2Zr_2O_7$	6990	1.08	1.16
$(Dy_{0.35}Er_{0.35}Sm_{0.1}Nd_{0.1}Yb_{0.1})_2Zr_2O_7$	7240	1.17	1.15
$(Dy_{0.2}Er_{0.2}Sm_{0.2}Nd_{0.2}Yb_{0.2})_2Zr_2O_7$	7150	1.15	1.15

Table A1
Relative densities (ratio of the measured Archimedes density and the theoretical density from lattice parameters) and grain sizes of the RE zirconates determined by the linear intercept method.

Composition	Relative Density (%)	Average Grain Size (μm)
$Nd_2Zr_2O_7$	93.4	0.85
$Sm_2Zr_2O_7$	95.2	0.76
$Gd_2Zr_2O_7$	91.9	0.55
$Dy_2Zr_2O_7$	81.1	0.35
$Er_2Zr_2O_7$	78.5	0.55
$Yb_2Zr_2O_7$	86.0	0.68
$(Gd_{0.4}Yb_{0.6})_2Zr_2O_7$	88.8	0.68
$(Gd_{0.55}Yb_{0.45})_2Zr_2O_7$	90.3	0.71
$(Gd_{0.7}Yb_{0.3})_2Zr_2O_7$	85.8	0.65
$(Gd_{0.85}Yb_{0.15})_2Zr_2O_7$	89.6	0.58
$(Gd_{0.7}Nd_{0.1}Sm_{0.1}Yb_{0.1})_2Zr_2O_7$	96.9	0.30
$(Gd_{0.25}Nd_{0.25}Sm_{0.25}Yb_{0.25})_2Zr_2O_7$	89.1	0.94
$(Dy_{0.35}Er_{0.35}Sm_{0.1}Nd_{0.1}Yb_{0.1})_2Zr_2O_7$	92.0	0.67
$(Dy_{0.2}Er_{0.2}Sm_{0.2}Nd_{0.2}Yb_{0.2})_2Zr_2O_7$	91.3	0.74

ions are due to electronic transitions that are shielded by the outer *5s* to *6s* electron orbitals, the absorptions of the different rare-earths are expected to be largely independent of one another when they are dissolved in the same host oxide. (There is some overlap, for instance between the *Er* $^4F_{13/2}$ and the *Yb* $^2F_{5/2}$ levels that is utilized in some compounds for frequency up-conversion [7]). To test the assumption of spectral independence, a polycrystalline gadolinium zirconate containing *Sm, Nd* and *Yb* ions was prepared. The hemispherical absorption spectrum of polycrystalline $(Gd_{0.7}Sm_{0.1}Nd_{0.1}Yb_{0.1})_2Zr_2O_7$ is shown in Fig. 5 with the peaks associated with the electronic transitions of the *Sm, Nd* and *Yb* ions colored to distinguish them. Comparison with the absorption spectra for the individual zirconates (Figs. 3 and 4) indicates that the absorption bands occur at the same wavelengths and are insensitive to the host. The breadth of the individual absorption bands is also similar. The spectral absorption coefficient of the mixed oxide zirconate is shown together with the absorption coefficients of a higher dopant concentration oxide, $(Gd_{0.25}Sm_{0.25}Nd_{0.25}Yb_{0.25})_2Zr_2O_7$. The spectral locations of the individual absorption bands are the same but, as expected, the absorption coefficients are larger.

In another test of the independence of the absorption from different rare-earth ions, a zirconate having five, equi-molar concentrations of different optical active rare-earth ions dissolved namely, $(Dy_{0.2}Er_{0.2}Sm_{0.2}Nd_{0.2}Yb_{0.2})_2Zr_2O_7$ was synthesized. As with the doped gadolinium zirconate, each absorption band can be identified with one or others of the individual rare-earth ions in solution, as indicated in Fig. 5(c), and no other absorption bands are observed.

4.2. Thermal conductivity

Unlike most oxides with simple crystal structures, such as alumina and magnesia [49], the thermal conductivity of the rare-earth zirconates do not exhibit the characteristic 1/T dependence decrease with increasing temperature, asymptotically approaching a plateau value at high temperatures, typically greater than twice the Debye temperatures. Rather, as shown in Figs. 6(a) and 6(b), their thermal conductivity is almost independent of temperature. For comparison, the data for the Yb_2O_3, Y_2O_3, and Al_2O_3, all three having the corundum crystal structure, are shown in Fig. 6(a). Notably, the thermal conductivities of all the individual rare-earth zirconates studied, as well as the mixed cation zirconates, including the equi-molar, "high-entropy" zirconate, are, within experimental measurement uncertainty, indistinguishable. At the

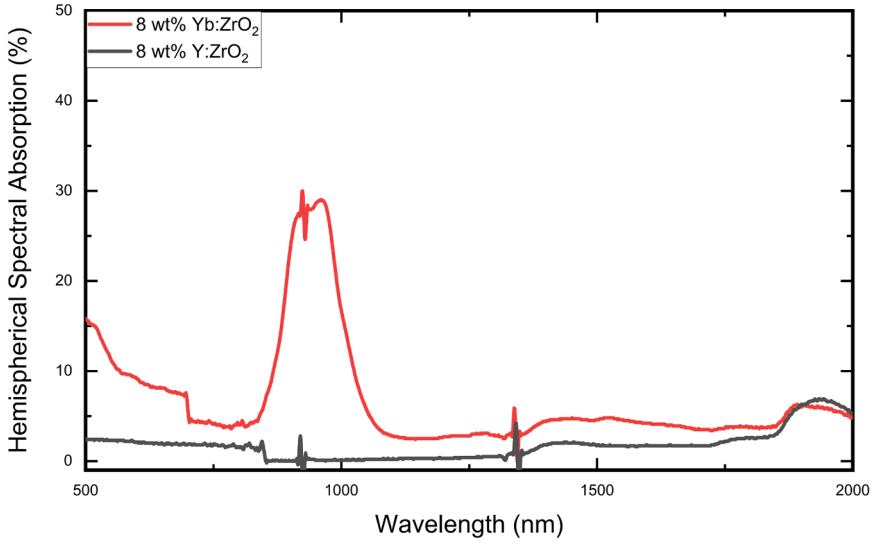

Fig. A1. Comparison of the spectral absorption of polycrystalline 8 w/o Yb_2O_3 doped zirconia and polycrystalline 8 w/o Y_2O_3 doped zirconia. The characteristic absorption due to the $^2F_{7/2} - {}^2F_{5/2}$ electronic transition, is observed in the Yb_2O_3 doped zirconia but not in the 8w/o Y_2O_3 in which Yb^{3+} is replaced by Y^{3+}. The absorption width is ~ 140 nm.

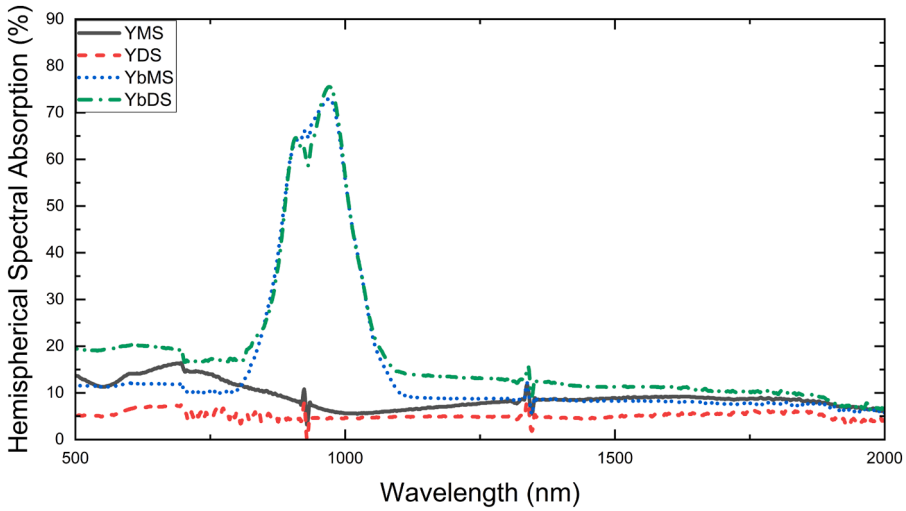

Fig. A2. Comparison of the hemispherical spectral absorption of polycrystalline Yb_2SiO_5 ytterbium monosilicate (YbMS), $Yb_2Si_2O_7$ ytterbium disilicate (YbDS) and their yttrium counterparts, Y_2SiO_5 (YMS) and $Y_2Si_2O_7$ (YDS).

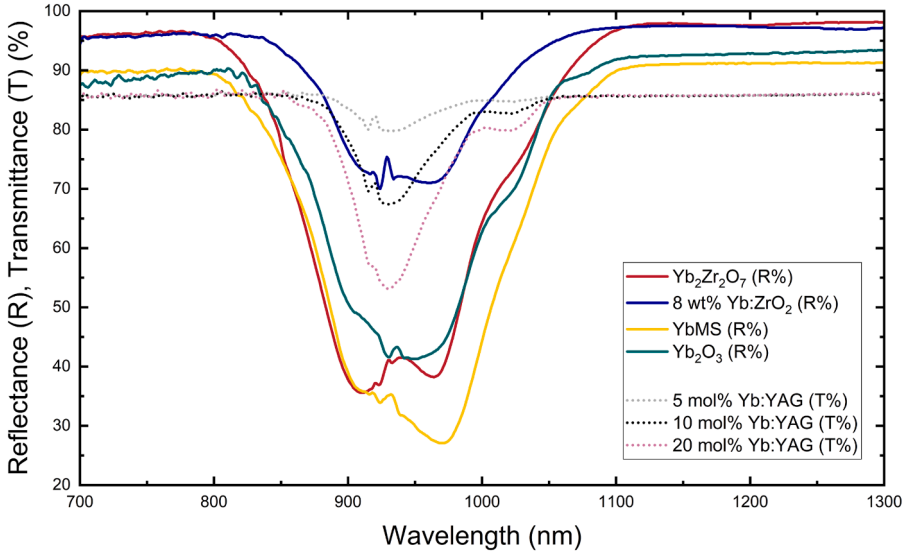

Fig. A3. The diffusive reflectance and transmittance spectra of several Yb^{3+} containing, polycrystalline oxide compounds illustrating the variation of the absorption peak positions and intensities on the Yb^{3+} ions' locations in the host lattice. Only the YAG single crystals exhibit a single absorption band.

higher temperatures, their values are also close to the high temperature minimum thermal conductivities, calculated from Eq. 2, (Table 2).

5. Discussion

The results presented here, and in the Appendices, clearly demonstrate that wavelength-selective oxide absorbers can be produced by doping a variety of refractory oxide hosts with specific rare-earth ions. In each composition studied, the absorption bands correspond to the allowed electronic transitions associated with the 4*f* electrons. This is consistent with the expectations of crystal field theory and the known absorption spectra from a variety of laser crystals, such as Sm:YAG and Nd:YAG [55]. In contrast to the design of phosphors, a much greater range of doping concentrations is achievable and, in the zirconates, can extend across the entire solid solution range. Significantly, the absorption from different rare-earth ions in solid solution in the same oxide is spectrally additive in the sense that the absorption wavelengths associated with the different rare-earth ions are independent of one another. Given that the origin of the absorption are electronic transitions shielded from the valence electrons primarily involved in bonding, this is not an unexpected finding, but it does provide an opportunity to design multiple doping schemes to match specific absorption spectra requirements in the visible and infrared, for instance, to design absorbers for high temperature emissions from water vapor and carbon dioxide. It is also found that the observed spectral absorption variations do not affect the already low, high-temperature thermal conductivity, within measurement uncertainty, so that the thermal and optical properties are largely independent of one another.

In the context of contemporary materials research, a considerable literature has developed concerning the beneficial effects of equi-molar and high-entropy compositions on mechanical properties of metallic alloys. Similar mixing of cations produces a reduction in the room temperature and intermediate temperature thermal conductivities of some oxides [49]. However, as shown here, and in previous work [56], no significant reduction in high temperature thermal conductivity is produced by this mixing. Nevertheless, as demonstrated in this work, the concept of high entropy mixing of different cations can be exploited to produce predictable and systematic variations in optical spectral

absorption, creating an additional dimension to the design of complex oxides rather than their elastic or thermal conduction properties. In the context of high temperature oxides, for instance in the design of thermal radiation barriers, the ability to modify the absorption coefficients in the thermal radiation window provides an opportunity to modify the radiative heat transfer through a coating independently of thermal conduction [4]. Further work is underway to quantify the temperature dependence of the absorption coefficients. When an electron is excited to a higher energy state by an incoming photon, there are two pathways to decaying to the ground state: by radiative processes which involve the emission of a photon and by non-radiative processes which involve the emission of a phonon. For TBC materials, the emission of a phonon is preferred because these are already low thermal conductivity materials which leads to a decrease in the total heat flux through the coating. Conveniently, photon to phonon conversion has been shown to become more efficient at higher temperatures [21].

In closing, the results of this work suggest that the same substitutional doping approach can be used to design, and create, high-emissivity, high-temperature oxides, and coatings for applications in the visible-near infra-red region. This expectation is based on the equivalence of the spectral emittance, ε (λ), of a thick coating being the same as its spectral absorptance, α (λ), usually expressed in terms of Kirchoff's law [57]. This equivalence has been demonstrated, for instance, by measurements of the rare-earth oxides, Er_2O_3, Sm_2O_3, Yb_2O_3, and Nd_2O_3. They exhibit high emittance at high temperatures [58] at the same wavelengths as they have high optical absorption at room temperatures. Experiments are underway to test this prediction and create new oxides (and silicates and carbides) that exhibit large values of spectral emittance in the "thermal radiation window" at very high temperatures.

6. Conclusions

We have demonstrated that substitutional doping of translucent oxides, such as zirconates, zirconia, and silicates with rare-earth cations can create selective absorbing materials in the visible/near IR spectral region. The absorption from different rare-earth ions in solid solution in the same oxide is spectrally additive. For the zirconates, we showed that the minimum thermal conductivity at high temperature is unaffected by rare-earth dopant even for equi-molar, high entropy compositions. This allows for the design of optical properties that are independent of thermal conduction properties. This has the potential for using substitutional doping in ceramics for many high temperature applications such as solar thermal collectors and advanced thermal barrier coatings.

Declaration of Competing Interest

The authors declare that they have no known competing financial interests or personal relationships that could have appeared to influence the work reported in this paper.

Acknowledgements

The work described was supported by ONR under grant N00014-21-1-2478. The work of Giovanni Pisaturo was part of his Masters' Thesis from ETH Switzerland.

Appendices

References

[1] T.H. Her, R.J. Finlay, C. Wu, S. Deliwala, E. Mazur, Microstructuring of silicon with femtosecond laser pulses, Appl. Phys. Lett. 73 (12) (1998) 1673–1675.
[2] S. Wijewardane, D.Y. Goswami, A review on surface control of thermal radiation by paints and coatings for new energy applications, Renew. Sustain. Energy Rev. 16 (4) (2012) 1863–1873.
[3] C. Tregambi, M. Triano, F. Montagnaro, R. Solimene, P. Saatino, Fluidized beds for concentrated solar thermal technologies - a review, Front. Energy Res. 9 (4) (2021).
[4] Q. Flamant, D.R. Clarke, Opportunities for minimizing radiative heat transfer in future thermal and environmental barrier coatings, Scr. Mater. 173 (2019) 26–31.
[5] D.C. Harris, Durable 3–5 μm transmitting infrared window materials, Infrared Phys. Technol. 39 (4) (1998) 185–201.
[6] D.C. Harris, Bellingham, WA. Materials for Infrared Windows and Domes: Properties and Performance, SPIE Press,, 1999.
[7] R.J.D. Tillney, Colour and the Optical Properties of Materials: An Exploration of the Relationship Between Light. the Optical Properties of Materials and Colour, 2 ed, John Wiley & Sons, Ltd,, Chichester, U.K., 2011.
[8] K. Nassau, The Physics and Chemistry of Color: The Fifteen Causes of Color, 1 ed., John Wiley & Sons,, New York, NY, 1983.
[9] D.M. Lipkin, D.R. Clarke, M. Hollatz, M. Bobeth, W. Pompe, Stress development in alumina scales formed upon oxidation of (111) NiAl single crystals, Corros. Sci. 39 (2) (1997) 231–242.
[10] B. Henderson, G.F. Imbusch, Optical Spectroscopy of Inorganic Solids, Clarendon Press,, Oxford, 1989.
[11] G. Blasse, B.C. Grabmaier, Luminescent Materials, Springer-Verlag,, Berlin Heidelberg, 1994.
[12] L. Wang, J.I. Eldridge, S.M. Guo, Thermal radiation properties of plasma-sprayed Gd2Zr2O7 thermal barrier coatings, Scr. Mater. 69 (9) (2013) 674–677.
[13] D.C. Harris, properties and performance. Materials for infrared windows and domes, SPIE Optical Engineering Press, Bellingham, Wash,, 1999.
[14] B. Henderson, G.F. Imbusch, Optical Spectroscopy of Inorganic Solids, Claredon Press,, 1989.
[15] R.G. Burns, Mineralogical Applications of Crystal Field Theory, 2 ed., Cambridge University Press,, Cambridge, U.K., 1993.
[16] G.H. Dieke, Spectra and Energy Levels of Rare Earth Ions in Crystals, Interscience Publishers,, New York, NY, 1968.
[17] A.R. West, Basic Solid State Chemistry, John Wiley,, 1984.
[18] Y.-M. Chiang, D. Birnie, W.D. Kingery, Physical Ceramics, John Wiley,, New York, 1997.
[19] R.D. Shannon, C.T. Prewitt, Effective ionic radii in oxides and fluorides, Acta Crystallogr. Sect. B 25 (5) (1969) 925–946.
[20] M. Kreye, K.D. Becker, An optical in-situ study of the re-oxidation kinetics of mixed valent Yb3Al5O12, Phys. Chem. Chem. Phys. 5 (11) (2003) 2283–2290.
[21] M.D. Chambers, D.R. Clarke, Doped oxides for high-temperature luminescence and lifetime thermometry, Annu. Rev. Mater. Res. 39 (1) (2009) 325–359.
[22] G.H. Dieke, H.M. Crosswhite, The spectra of the doubly and triply ionized rare earths, Appl. Opt. 2 (7) (1963) 675–686.
[23] D.-J. Kim, Effect of Ta2O5, Nb2O5, and HfO2 Alloying on the Transformability of Y2O3-Stabilized Tetragonal ZrO2, J. Am. Ceram. Soc. 73 (1) (1990) 115–120.
[24] F.M. Pitek, C.G. Levi, Opportunities for TBCs in the ZrO2–YO1.5–TaO2.5 System, Surf. Coat. Technol. 201 (12) (2007) 6044–6050.
[25] J.S. Van Sluytman, S. Krämer, V.K. Tolpygo, C.G. Levi, Microstructure evolution of ZrO2–YbTaO4 thermal barrier coatings, Acta Mater. 96 (2015) 133–142.
[26] Y. Shen, R.M. Leckie, C.G. Levi, D.R. Clarke, Low thermal conductivity without oxygen vacancies in equimolar YO1.5 + TaO2.5- and YbO1.5 + TaO2.5-stabilized tetragonal zirconia ceramics, Acta Mater. 58 (13) (2010) 4424–4431.
[27] M. Gurak, Q. Flamant, L. Laversenne, D.R. Clarke, On the Yttrium Tantalate - Zirconia phase diagram, J. Eur. Ceram. Soc. 38 (9) (2018) 3317–3324.
[28] D.R. Clarke, C.G. Levi, A.G. Evans, Enhanced zirconia thermal barrier coating systems, Proc. Inst. Mech. Eng. Part a-J. Power Energy 220 (A1) (2006) 85–92.
[29] D.R. Clarke, M. Oechsner, N.P. Padture, Thermal-barrier coatings for more efficient gas-turbine engines, MRS Bull. 37 (10) (2012) 891–898.
[30] J. Chevalier, L. Gremillard, A.V. Virkar, D.R. Clarke, The tetragonal-monoclinic transformation in zirconia: lessons learned and future trends, J. Am. Ceram. Soc. 92 (9) (2009) 1901–1920.
[31] D.R. Clarke, S.R. Phillpot, Thermal barrier coating materials, Mater. Today 8 (6) (2005) 22–29.
[32] J. Callaway, H.C. von Baeyer, Effect of point imperfections on lattice thermal conductivity, Phys. Rev. 120 (4) (1960) 1149–1154.
[33] A.M. Hofmeister, J.M. Branlund, M. Pertermann, 2.19 - Properties of Rocks and Minerals – Thermal Conductivity of the Earth, in: G. Schubert (Ed.). Treatise on Geophysics, Elsevier,, Amsterdam, 2007, pp. 543–577.
[34] D.G. Cahill, S.K. Watson, R.O. Pohl, Lower limit to the thermal conductivity of disordered crystals, Phys. Rev. B 46 (1992) 6131–6140.
[35] D.R. Clarke, Materials selection guidelines for low thermal conductivity thermal barrier coatings, Surf. Coat. Technol. 163 (2003) 67–74.
[36] C. Kittel, Introduction to solid state physics, 8th ed., J. Wiley,, Hoboken, NJ, 2005.
[37] J.P. Jolivet, M. Henry, J. Livage, Metal Oxide Chemistry and Synthesis: From Solution to Solid State, John Wiley and Sons,, 2000.
[38] E.L. Pang, C.A. McCandler, C.A. Schuh, Reduced cracking in polycrystalline ZrO2-CeO2 shape-memory ceramics by meeting the cofactor conditions, Acta Mater. 177 (2019) 230–239.
[39] H.G. Hecht, The interpretation of diffuse reflectance spectra, Natl. Bur. Stand. (1976).
[40] J.C. Richmond, Relation of emittance to other optical properties, J. Res. Natl. Bur. Stand. C. Eng. Instrum. 67C (3) (1963) 217.
[41] W.J. Parker, R.J. Jenkins, C.P. Butler, G.L. Abbott, Flash method of determining thermal diffusivity, heat capacity, and thermal conductivity, J. Appl. Phys. 32 (9) (1961) 1679–1684.

[42] C.E. Wicks, Thermodynamic properties of 65 elements: their oxides, halides, carbides and nitrides, by C. E. Wicks, and F. E. Block, U.S. Govt. Print. Off., (1963), District of Columbia, 1963.
[43] L.B. Pankratz, E.G. King, HIGH-TEMPERATURE HEAT CONTENTS AND ENTROPIES OF THE SESQUIOXIDES OF ERBIUM, HOLMIUM, THULIUM, AND YTTERBIUM, (1962).
[44] Y. Zhang, I.-H. Jung, Critical evaluation of thermodynamic properties of rare earth sesquioxides (RE = La, Ce, Pr, Nd, Pm, Sm, Eu, Gd, Tb, Dy, Ho, Er, Tm, Yb, Lu, Sc and Y), Calphad 58 (2017) 169–203.
[45] O. Fabrichnaya, M.J. Kriegel, J. Seidel, G. Savinykh, L.P. Ogorodova, I.A. Kiseleva, H.J. Seifert, Calorimetric investigation of the $La_2Zr_2O_7$, $Nd_2Zr_2O_7$, $Sm_2Zr_2O_7$ and $LaYO_3$ compounds and CALPHAD assessment of the La_2O_3–Y_2O_3 system, Thermochim. Acta 526 (1) (2011) 50–57.
[46] H.J. Schugar, E.I. Solomon, W.L. Cleveland, L. Goodman, Simultaneous pair electronic transitions in ytterbium oxide, J. Am. Chem. Soc. 97 (22) (1975) 6442–6450.
[47] G. Boulon, Y. Guyot, H. Canibano, S. Hraiech, A. Yoshikawa, Characterization and comparison of Yb3+-doped YA1O3 perovskite crystals (Yb:YAP) with Yb3+-doped Y3Al5O12 garnet crystals (Yb:YAG) for laser application, J. Opt. Soc. Am. B Opt. Phys. 25 (5) (2008) 884–896.
[48] W.B. White, Diffuse-reflectance spectra of rare-earth oxides, Appl. Spectrosc. 21 (3) (1967) 167–171.
[49] W.D. Kingery, Thermal conductivity: XIV, conductivity of multicomponent systems, J. Am. Ceram. Soc. 42 (12) (1959) 617–628.
[50] W.D. Kingery, J. Francl, R.L. Coble, T. Vasilos, Thermal Conductivity: X, Data for Several Pure Oxide Materials Corrected to Zero Porosity, J. Am. Ceram. Soc. 37 (2) (1954) 107–110.
[51] A.M. Limarga, D.R. Clarke, The grain size and temperature dependence of the thermal conductivity of polycrystalline, tetragonal yttria-stabilized zirconia, Appl. Phys. Lett. 98 (21) (2011), 211906.
[52] J. Wu, X. Wei, N.P. Padture, P.G. Klemens, M. Gell, E. García, P. Miranzo, M. I. Osendi, Low-thermal-conductivity rare-earth zirconates for potential thermal-barrier-coating applications, J. Am. Ceram. Soc. 85 (12) (2002) 3031–3035.
[53] Z.-G. Liu, J.-H. Ouyang, Y. Zhou, J. Li, X.-L. Xia, Influence of ytterbium- and samarium-oxides codoping on structure and thermal conductivity of zirconate ceramics, J. Eur. Ceram. Soc. 29 (4) (2009) 647–652.
[54] Q. Xu, W. Pan, J. Wang, C. Wan, L. Qi, H. Miao, K. Mori, T. Torigoe, Rare-earth zirconate ceramics with fluorite structure for thermal barrier coatings, J. Am. Ceram. Soc. 89 (1) (2006) 340–342.
[55] L.D. DeLoach, S.A. Payne, L.L. Chase, L.K. Smith, W.L. Kway, W.F. Krupke, Evaluation of absorption and emission properties of Yb^{3+} doped crystals for laser applications, IEEE J. Quantum Electron. 29 (4) (1993) 1179–1191.
[56] M.R. Winter, D.R. Clarke, Oxide materials with low thermal conductivity, J. Am. Ceram. Soc. 90 (2) (2007) 533–540.
[57] T.L. Bergman, Introduction to heat transfer, 6th ed., John Wiley & Sons, Inc,, Hoboken, NJ, 2011.
[58] G.E. Guazzoni, High-temperature spectral emittance of oxides of erbium, samarium, neodymium and ytterbium, Appl. Spectrosc. 26 (1) (1972) 60–65.